Thermodynamics of stable nanocrystalline alloys: A Monte Carlo analysis

Citation: Chookajorn, Tongjai, and Christopher A. Schuh. "Thermodynamics of stable nanocrystalline alloys: A Monte Carlo analysis." Phys. Rev. B 89, 064102 (February 2014). © 2014 American Physical Society

As Published: http://dx.doi.org/10.1103/PhysRevB.89.064102

Publisher: American Physical Society

Persistent URL: http://hdl.handle.net/1721.1/88736

Version: Final published version: final published article, as it appeared in a journal, conference proceedings, or other formally published context

Thermodynamics of stable nanocrystalline alloys: A Monte Carlo analysis

Tongjai Chookajorn and Christopher A. Schuh*
Department of Materials Science and Engineering, Massachusetts Institute of Technology, 77 Massachusetts Avenue, Cambridge, Massachusetts 02139, USA
(Received 2 June 2013; published 5 February 2014)

A Monte Carlo simulation method is used to study the energetics and configuration of binary alloys when grain boundary states are included as potential equilibrium features. For certain sets of alloy properties, a nanostructured grain assembly is found to be the most energetically favorable state, and is stabilized by grain boundary segregation of solute. The conditions for stability against grain coarsening and the "grain boundary energy" requirement are clarified, with emphasis on the closed system conditions that prevail in nanostructured alloys. Two thermodynamic parameters, the grain boundary area potential and the grain boundary formation energy, are quantitatively disentangled and shown to differently reflect grain stability and the energy state of interfaces. These discussions provide insights on how alloying can be used to actively manipulate nanocrystalline grain sizes.

DOI: 10.1103/PhysRevB.89.064102 PACS number(s): 61.46.−w, 61.72.Mm, 64.75.Jk, 81.05.Bx

I. INTRODUCTION

Even though nanoscale grain sizes can be fairly easily achieved in many polycrystalline materials, nanostructure stability is a primary concern for subsequent processing and usage. Because of their high volume fraction of high-energy grain boundaries, nanocrystalline materials are generally unstable against grain coarsening. Alloying has been identified as a means of stabilizing the structure, and not only in a kinetic, grain boundary pinning sense, but also from a perspective of thermodynamic energy minimization. Following Weissmuller [1,2], the free energy G of a polycrystal at constant pressure and temperature can be written as a sum of chemical potential and interface terms,

$$G = \Sigma \mu_i N_i + \gamma A, \tag{1}$$

where N is the number of atoms of chemical type "i" with the chemical potential μ_i, and A is the total grain boundary area with the associated grain boundary formation energy of γ per unit area. The stability of a grain structure is evaluated by considering the derivative of the free energy with respect to the change in total grain boundary area:

$$\frac{dG}{dA} = \frac{d(\Sigma \mu_i N_i)}{dA} + A\frac{d\gamma}{dA} + \gamma. \tag{2}$$

For pure materials, the free energy is $G = \mu N + \gamma_0 A$, and the derivative is simply $\frac{dG}{dA} = \gamma_0$. As a result, the system free energy can be lowered by decreasing the total grain boundary area until the grain structure is completely coarsened to a single-crystal ground state. On the other hand, for alloyed materials the derivative can be further expanded to

$$\frac{dG}{dA} = \frac{d(\Sigma \mu_i N_i)}{dX_c}\frac{dX_c}{dA} + A\frac{d\gamma}{dX_c}\frac{dX_c}{dA} + \gamma, \tag{3}$$

where X_c is the solute concentration in crystal, or the grain interior.

The derivative $\frac{dG}{dA}$ evaluates differently in open and closed systems. For open systems, the grain interior concentration X_c is kept constant and therefore $\frac{dG}{dA} = \gamma$. Both of these terms, $\frac{dG}{dA}$ and γ, have units of energy per unit area, and both have been called "grain boundary energy" in the literature. For open systems, this is appropriate given their equivalence. However, for closed systems, these quantities are not equal, and thus different nomenclature is required. Terms such as "open-system grain boundary energy" or "grain boundary formation energy" are appropriate for γ, and in a closed system it has been pointed out that this quantity can even be negative for some grain boundary solute segregation states [1–7]. The quantity $\frac{dG}{dA}$ is the more important term for identifying an equilibrium grain size, which occurs when $\frac{dG}{dA} = 0$ but not necessarily when $\gamma = 0$. We call $\frac{dG}{dA}$ the "grain boundary area potential."

In the dilute limit of McLean-type grain boundary segregation, an alloying element can lower the energy penalty of grain boundaries via

$$\gamma(X) = \gamma_0 - \Gamma(\Delta H^{seg} + kT \ln X), \tag{4}$$

where Γ is the specific solute excess at the grain boundaries, ΔH^{seg} is the dilute-limit enthalpy of grain boundary segregation, k is the Boltzmann constant, T is the absolute system temperature, and X is the global solute content. According to Eq. (4), grain boundary energetics, and therefore nanostructure stability, can be modified via alloying and the effective grain boundary formation energy after alloying is dictated by the added solute content. Accordingly, the grain boundary area potential of a dilute polycrystalline alloy can be expressed as a function of solute characteristics and concentration by combining Eqs. (2) and (4) as

$$\frac{dG}{dA} = \frac{d(\Sigma \mu_i N_i)}{dA} + \gamma_0 - \left(\Gamma + A\frac{d\Gamma}{dA}\right)(\Delta H^{seg} + kT \ln X). \tag{5}$$

For alloy systems with positive grain boundary adsorption, $\frac{dG}{dA}$ can be suppressed to zero or a negative value by maintaining a sufficient solute excess at the grain boundaries with respect to the change in grain size ($\Gamma > -A\frac{d\Gamma}{dA}$), and a free energy minimum at $\frac{dG}{dA} = 0$ can be accessed with a specific grain boundary segregation-grain size state (Γ,A).

*schuh@mit.edu

Early discussions of this concept include those by Weissmuller [1,2] and Kirchheim [8–10], among others [5,6,11–15], and focus exclusively on the ability of grain boundary segregation to stabilize a nanocrystalline alloy against grain growth, i.e., $\frac{dG}{dA} = 0$ is the only consideration of equilibrium. More recently, we have proposed that solid solutions with solute segregation to grain boundaries can, moreover, constitute formal ground-state structures for the alloy system, making some nanostructured alloys not only stable against grain growth, but against phase separation as well [16]. Following that first report, Murdoch and Schuh [17] used analytical thermodynamic free energy functions to evaluate a variety of possible stable nanostructures. They identified some sets of alloy energetic parameters for which a stable, single-phase solid solution with a nanocrystalline structure could be the system ground state, with solute segregation at grain boundaries. They also proposed that several new stable nanostructures may be possible in systems with a propensity for grain boundary segregation, including dual-phase nanocrystalline structures, amorphous structures (comprising all "intergranular" alloy matter), metastable nanocrystalline structures that resist grain growth but not phase separation, and also regimes where more than one of the above states may coexist.

In this paper, we take another step to elucidate nanostructural alloy ground states, in systems where alloy configuration and grain boundary content are both treated as variables. Specifically, we develop a lattice Monte Carlo approach in which both features of the problem are included, offering insight on the accessible ground states and complex alloy configurations that may be expected in nanostructured systems. These simulation results also provide some clarification on the grain boundary energy requirement for grain stability, which for a closed system has nuances that can run against intuition in some cases.

II. SIMULATION PROCEDURE

Lattice-based Monte Carlo (MC) methods have been widely applied to both alloying thermodynamics and grain structure problems [18–34]. To capture the interaction between solute and solvent in a polycrystalline environment and their effects on stabilizing nanostructured grains, we use a lattice MC method that tracks both atomic chemical identity and grain allegiance at every lattice point. As a simplifying first step, only phase separating binary alloys (i.e., those with positive enthalpies of mixing) are considered, and a body centered cubic (BCC) lattice, as in Fig. 1 is used. Each atomic site is assigned an atom type, which denotes the chemical identity of the atom as solvent (A) or solute (B), and a grain number, which differentiates atoms in the same grain from those that are neighbors across grain boundaries. Periodic boundary conditions are applied on all three principal axes. For ease of viewing in what follows, we present two-dimensional sections viewed along the [001] direction, with atoms in both the sectioning plane and first subsurface plane visible.

A. Bond energy calculation

Our simulation is based on nearest-neighbor interactions only, with six unique bond types: between each pairing of the atomic types (A and B) and lying either in the grain interior or across a grain boundary (i.e., matched or unmatched grain numbers, respectively). The total internal energy U is calculated by summing the bond energy between all atoms:

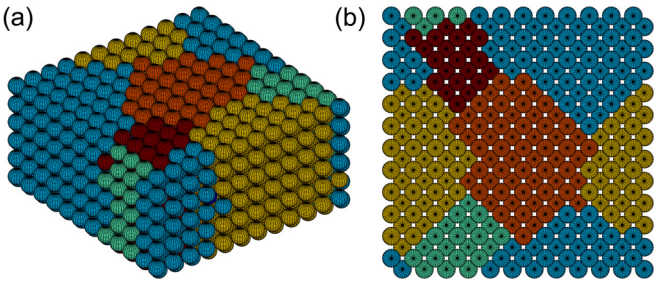

FIG. 1. (Color online) Representative lattice of a polycrystalline structure produced by the Monte Carlo simulation. (a) A three-dimensional view of a BCC lattice with $12 \times 12 \times 12$ atoms is shown with (b) the top down view along the [001] direction, revealing the top two atomic planes. The atoms with the same color belong to the same grain.

$$U = \sum_{\text{all bonds}} \left[\left(N_c^{AA} E_c^{AA} + N_c^{BB} E_c^{BB} + N_c^{AB} E_c^{AB} \right) + \left(N_{gb}^{AA} E_{gb}^{AA} + N_{gb}^{BB} E_{gb}^{BB} + N_{gb}^{AB} E_{gb}^{AB} \right) \right], \quad (6)$$

where N is the number of bonds and E is the bond energy. The subscript denotes whether the bond is in a crystal (or grain interior, denoted by c) or across a grain boundary (denoted by gb), and the superscript denotes the chemical pairings involved. The internal energy can also be expressed as $U = \Sigma \mu_i N_i + \gamma A - PV + TS$, and at constant pressure P, volume V, temperature T, and entropy S, its derivative with respect to the change in total grain boundary area, $\frac{dU}{dA} = \frac{d(\Sigma \mu_i N_i + \gamma A)}{dA}$, is equivalent to the grain boundary area potential as defined earlier in Introduction.

There are six independent bond energy inputs to our model or five if one of the bond types is regarded as the reference state that sets the temperature scale. This multidimensional parameter space offers great flexibility for modeling various alloy systems, but its breadth is too large to consider systematically in detail here. For purposes of simplifying the parameter space, it is useful to connect the bond energies to more routine macroscopic material parameters. These include the pure component A grain boundary formation energy:

$$\gamma_0^A = \frac{zt}{2\Omega^A} \left(E_{gb}^{AA} - E_c^{AA} \right), \quad (7)$$

and an equivalent expression for the pure component B grain boundary formation energy, as well as the alloy enthalpy of mixing:

$$\Delta H^{mix} = z \omega_c X (1 - X), \quad (8)$$

and the dilute-limit enthalpy of grain boundary segregation:

$$\Delta H^{seg} = z \left[\omega_c - \frac{\omega_{gb}}{2} - \frac{1}{2zt} \left(\Omega^B \gamma_0^B - \Omega^A \gamma_0^A \right) \right], \quad (9)$$

which inherently incorporates various effects such as chemical interactions, difference in interface energies, and solute-solvent size mismatch (elastic energy), as described by the

linear combination of subcontributions:

$$\Delta H^{\text{seg}} = \Delta E_{\text{chemical}} + \Delta E_{\text{interface}} + \Delta E_{\text{elastic}}. \quad (10)$$

Although in what follows we will exercise the model in its most general form, without considering the details of these various contributions, it is important to note that the connection to these classical views of grain boundary segregation is seamless. The model can be provided inputs by beginning with a specific alloy system for which the chemical energies, surface energies, size mismatch, etc., are known, and using Eq. (10) to evaluate the required input value of ΔH^{seg}.

In these equations, $\omega_c = E_c^{AB} - (\frac{E_c^{AA}+E_c^{BB}}{2})$, is the regular solution grain interaction energy, $\omega_{gb} = E_{gb}^{AB} - (\frac{E_{gb}^{AA}+E_{gb}^{BB}}{2})$, is the grain boundary interaction energy, z is the coordination number, t is the grain boundary thickness, taken as 0.5 nm throughout, and Ω is the atomic volume.

The number of independent parameters can be reduced by focusing strictly on mixing thermodynamics, i.e., by assuming equal like-bond energies in the grain interior, $E_c^{AA} = E_c^{BB}$, and similar grain boundary penalties, $\frac{2\Omega^A\gamma_0^A}{zt} = \frac{2\Omega^B\gamma_0^B}{zt}$. These parameters are taken to be 1.26 and 0.05 eV/bond, respectively; they are selected for their match with the material parameters of tungsten metal for use in future work, but for the purposes of the present paper, can be regarded as essentially arbitrary. There remains only the temperature plus two independent adjustable bonding parameters, represented by the mixing parameters for grain and grain boundary regions: ω_c and ω_{gb}, which simply map to the more intuitive parameters, ΔH^{mix} and ΔH^{seg}, using $\Delta H^{\text{mix}} = z\omega_c$. Consequently, we can use a two-dimensional material parameter space such as in Fig. 2 to represent binary alloy systems based on their mixing and grain boundary segregation characteristics.

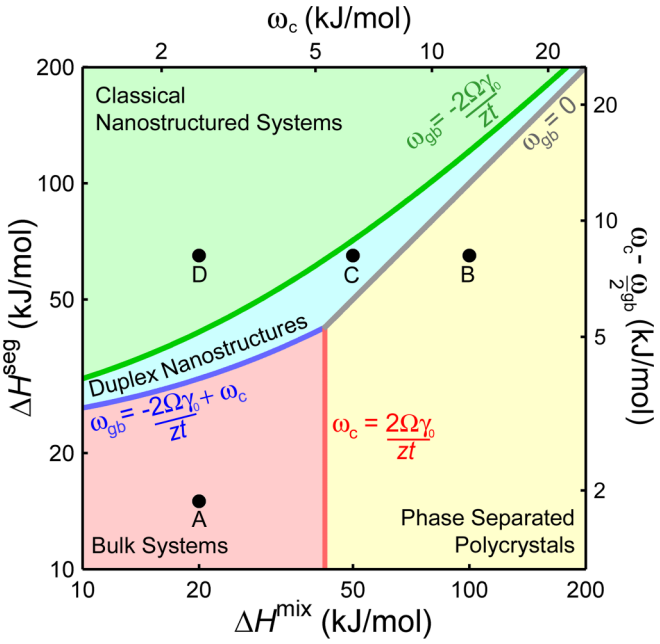

FIG. 2. (Color online) Nanostructure stability map for binary alloys with four boundary lines and four behavioral regimes.

The state space in Fig. 2 is similar to that presented in our earlier work [16] and in that of Murdoch and Schuh [17]. In the present case, this space can be understood in terms of the different bond types that are preferred in various regions of the map. Specifically, we identify four main regions that emerge from consideration of the bonding energies used in our MC model, and which are divided by the following boundary lines.

1. *Onset of solute segregation at grain boundaries,* $\omega_{gb} = 0$

The most important consideration for the present work is whether or not grain boundary solute segregation will occur, opening the door to stable nanostructures. Relief of interface energy penalty by grain boundary segregation requires a negative ω_{gb}, and the boundary line at $\omega_{gb} = 0$ along the diagonal of the map in Fig. 2, with negative ω_{gb} lying above the boundary line (or $\Delta H^{\text{seg}} > \Delta H^{\text{mix}}$), represents the cases where alloying can lower the grain boundary formation energy compared to its single-component counterpart.

2. *Transition from solid solution to grain boundary segregation,* $\omega_{gb} = -\frac{2\Omega^A\gamma_0^A}{zt} + \omega_c$

Even if ω_{gb} is negative and alloying lowers the grain boundary penalty, a bulk solid solution may yet be more stable than a grain boundary segregated state. Only when E_{gb}^{AB} is lower than E_c^{AB} would alloying be able to provide a lower-energy grain boundary state than a bulk solid solution. This occurs when the following inequality is met: $\omega_{gb} < -\frac{2\Omega^A\gamma_0^A}{zt} + \omega_c$.

3. *Onset of grain metastability,* $\omega_c = \frac{2\Omega^A\gamma_0^A}{zt}$

For those cases where grain boundary solute segregation is not preferred (i.e., lying in the lower part of Fig. 2), the structure will not have a stable nanostructure. The ground state in this condition could be a solid solution or a bulk phase separated state. The vertical boundary line in Fig. 2 represents the crossover between dominance of E_c^{AB} and E_{gb}^{AA} and therefore whether formation of solid solution in the grain interior or a single-component grain boundary results in a higher energy state. Solute precipitation becomes more likely with higher ω_c, and when $\omega_c > \frac{2\Omega^A\gamma_0^A}{zt}$, the system can lower the energy by forming a precipitated polycrystalline structure rather than a single-crystal solid solution.

4. *Onset of grain boundary stabilization,* $\omega_{gb} = -\frac{2\Omega^A\gamma_0^A}{zt}$

The last boundary line represents the ideal case where alloying can lower the grain boundary energy penalty sufficiently enough that a nanocrystalline structure becomes the system's ground state. This requires the alloyed grain boundaries to be the lowest-energy bonding state; such condition is realized only when $\omega_{gb} < -\frac{2\Omega^A\gamma_0^A}{zt}$, which defines the upper, green-shaded region in Fig. 2.

The above boundary lines construct the diagram in Fig. 2, and delineate four main regions worthy of further exploration using the MC model. We select four particular alloy systems, labeled A to D on the stability map in Fig. 2, to represent the regions enclosed by the four boundary lines. These are denoted as region A: bulk systems, region B: phase-separated polycrystals, region C: duplex nanostructures, and region D:

classical nanostructured systems and will be explored in more detail in later sections.

B. Monte Carlo procedure

Our Monte Carlo procedure is standard in the sense that we probe configuration space through individual switching events that are accepted if energy lowering and accepted with probability $P = e^{\frac{-(E_2-E_1)}{kT}}$ if energy raising; E_1 and E_2 are, respectively, the total system energies before and after the switch. There are two types of switching events in our MC procedure, considered as independent and referred to as grain switching and atom switching. A type of switch is first selected with equal probability. For atom switching, a solute atom and a solvent atom are selected at random (regardless of their grain numbers), and their chemical types are exchanged with the original grain number of each atomic site unchanged. For grain switching, an atom is chosen at random, and if it has at least one neighbor of a different grain number, its grain number is changed. The new grain number is chosen at random from among those of its nearest neighbors as well as a unique grain number that matches none of the neighboring atoms. Thus the grain switching event allows atoms at grain boundaries to change their grain allegiance, or to spontaneously nucleate new grains, which may subsequently grow or disappear.

The system is initialized at 10 000 K, where it is randomized, and then slowly cooled at a rate $\frac{-(T_{\text{step}}-T_{\text{final}})}{1000}$. The system spends one MC step at an immediate temperature, T_{step}, and cooling decelerates as the system temperature converges to the final target, T_{final}. The Monte Carlo procedure proceeds until the total system energy reaches a steady state. All simulations are performed for 100 000 MC steps, with each step corresponding to an average of one switch event per atom across the whole system. We tested this MC procedure for path independence by using different initial states (including bicrystal, polycrystal, amorphous, mixed, and unmixed) and establishing convergence to the same steady-state structure regardless of the initial grain structure and atomic distribution. We also verified that the rate of cooling specified above yielded sufficiently equilibrated structures for the conditions presented, by running various simulations at various rates and obtaining the same results.

C. Grain boundary segregation

To verify conformity of the present model to conventional grain boundary segregation thermodynamics, we perform some simulations on bicrystal geometries in which the grain numbers are fixed, so as to permit grain boundary segregation to develop independently of any change in grain structure. In the dilute limit, the enthalpy of grain boundary segregation relates to local solute concentrations, X_{gb} in the grain boundaries, and X_{c} in the grain interior, via the McLean segregation isotherm:

$$\frac{X_{\text{gb}}}{1-X_{\text{gb}}} = \frac{X_{\text{c}}}{1-X_{\text{c}}}\exp\left(\frac{E_{\text{diff}}}{kT}\right), \tag{11}$$

where E_{diff} is the energy difference between a solute atom residing in the grain interior with respect to a grain boundary. For a BCC bicrystal conjoined on the (001) planes, $E_{\text{diff}} = 8E_{\text{c}}^{\text{AB}} - (4E_{\text{gb}}^{\text{AB}} + 4E_{\text{c}}^{\text{AB}})$, which is equal to ΔH^{seg} when ΔH^{mix} and γ_0 are taken as zero to eliminate the effects from chemical mixing and grain boundary energy penalty.

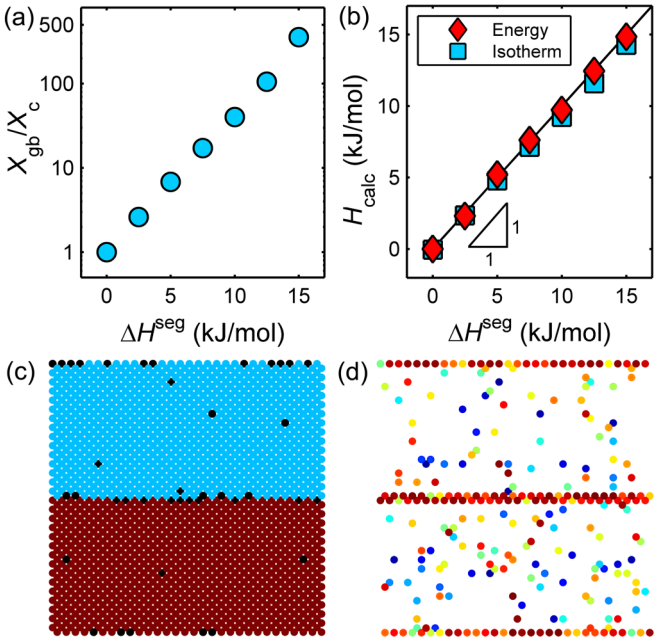

FIG. 3. (Color online) (a) The relative solute excess at grain boundaries in a bicrystal shows a higher tendency for grain boundary segregation with increasing ΔH^{seg}. (b) The energy difference calculated using the grain boundary segregation isotherm and the change in system energy both show the expected relationship with the input ΔH^{seg}. (c) A side view of a 30 × 30 × 60 BCC bicrystal with 2 at.% solute and $\Delta H^{\text{seg}} = 15$ kJ/mol. The color denotes the grain numbers and the black circles represent the solute atoms. (d) A solute distribution map of the same BCC bicrystal with the color of the solute atoms indicating the depth into the page. All simulations are performed at $T = 25$ °C.

The relative solute excess at grain boundaries, $X_{\text{gb}}/X_{\text{c}}$, is calculated from a bicrystal with $X = 0.1$–2 at.% and plotted with ΔH^{seg} in Fig. 3(a), along with a side view of the bicrystal [Fig. 3(c)] and a three-dimensional solute distribution map showing the solute atoms preferentially segregating at grain boundaries [Fig. 3(d)]. The energy difference E_{diff} after equilibrating the alloy configuration, denoted by H_{calc} in Fig. 3(b), displays the expected behavior. Alternatively, by definition E_{diff} can be calculated from the change in system energy normalized by the change in the number of solute atoms relocated to the grain boundaries after equilibration. This method reproduces the same relationship with ΔH^{seg}.

The change in grain boundary segregation behavior with solute content is further explored, to verify that the segregation tendency decreases as the boundary saturates with solute, as captured, for instance, by the Fowler-type isotherm common in interfacial segregation theory. Using a fixed value of $\Delta H^{\text{seg}} = 10$ kJ/mol, we repeat the above exercise for a range of solute contents $X = 0.1$–40 at.%. The effective segregation energy, H_{calc}, is calculated from the relative solute excess at grain boundaries using Eq. (11) and plotted with the global solute composition in Fig. 4. At dilute concentrations, H_{calc} matches the dilute-limit input ΔH^{seg}

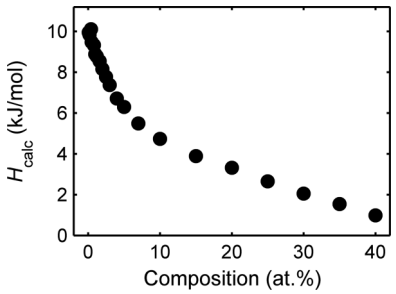

FIG. 4. Variation between effective grain boundary segregation energy and global solute content. All simulations are performed at $T = 25\,^{\circ}\mathrm{C}$ on a $30 \times 30 \times 60$ BCC bicrystal with $\Delta H^{\mathrm{seg}} = 10\,\mathrm{kJ/mol}$.

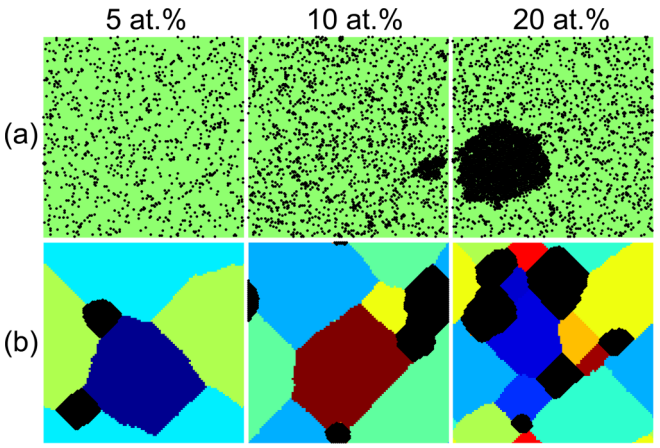

FIG. 5. (Color online) Systems with no stable nanostructured state at 500 °C from a $100 \times 100 \times 6$ BCC lattice. (a) System "A" with $\Delta H^{\mathrm{mix}} = 20\,\mathrm{kJ/mol}$ and $\Delta H^{\mathrm{seg}} = 15\,\mathrm{kJ/mol}$ forms single-crystalline solid solutions with precipitation emerging at 10 at.% solute concentration. (b) System "B" with $\Delta H^{\mathrm{mix}} = 100\,\mathrm{kJ/mol}$ and $\Delta H^{\mathrm{seg}} = 65\,\mathrm{kJ/mol}$ exhibits phase separation with no solute segregation at grain boundaries.

value of 10 kJ/mol, and this value declines monotonically at higher solute content. The form of the trend in Fig. 4 aligns with expectations, and highlights that composition dependence of the segregation energy is an emergent behavior that arises from solute-solute interactions; no additional new thermodynamic inputs are required to model nondilute behavior. Although the model takes a "dilute-limit" segregation energy as input, it is applicable beyond the dilute limit with no modification because it captures these collective effects. We conclude that conventional grain boundary segregation behavior is well captured by our simulation in both dilute and nondilute limits with proper composition dependence.

III. SYSTEMS WITHOUT STABLE NANOSTRUCTURED STATES

As described above, we will explore the basic behaviors of our model by examining in detail four case studies (A–D) that are typical of the kinds of equilibria we find with many varieties of inputs. These four cases lie in separate regions of Fig. 2, and in this section we begin with a brief examination of the first two structures, labeled A and B. These structures are similar in that they involve systems where grain boundary segregation is not expected to be energy lowering, and they exhibit bulk ground states.

Depending on the relative severity of the phase separation tendency and the grain boundary energy penalty, instability can manifest in several ways including the structures in Fig. 5, all of which have no apparent solute segregation at grain boundaries. For structure A, at low ΔH^{mix} and ΔH^{seg}, the grain boundary energy penalty is greater than the enthalpic terms and therefore all grain boundaries are higher in energy than grain interior bonds. A nanostructure cannot be maintained in this "bulk system" regime, highlighted in red in Fig. 2. The representative alloy system A in Fig. 5(a) displays bulk solid solution structures at low solute concentrations, and precipitation emerges at higher alloy contents beyond the solubility limit; in all cases, the system has only a single grain once equilibrated.

For structure B in Fig. 5(b), the system equilibrates to a polycrystal with phase separation. Although there are grain boundaries present, they are not decorated with solute in concentrations above those in the bulk solution. In this regime, highlighted in yellow in Fig. 2, the single-component grain boundaries have a bond energy with a magnitude between that of the bulk solid solution $E_{\mathrm{c}}^{\mathrm{AB}}$ and bulk phase separation $E_{\mathrm{c}}^{\mathrm{AA}}$ bonds. As a result, bulk phase separation is the preferred condition, but single-component grain boundaries may persist in an entropically stabilized condition.

Traversing from lower right to upper left in Fig. 2, there is a transition between the bulk-stable conditions described above and the green region where nanocrystalline structures may emerge. The blue region in which alloy C resides is a transition region between these behaviors; here the solute-segregated grain boundary is a low-energy configuration compared to unalloyed grain boundaries, but higher in energy compared to bulk phase separation. The "duplex nanostructures" from alloy C, shown in Fig. 6, display a nanocrystalline structure at low solute concentrations and become a duplex nanocrystalline structure with solvent-rich and solute-rich crystalline regions and solute segregation at grain boundaries at higher solute concentrations. These transitional structures may be better appreciated once a clearer understanding of the stable nanostructure region is reached, and we turn our attention to this in the following.

IV. CLASSICAL NANOSTRUCTURED SOLID SOLUTIONS

Alloying can lower the energy penalty of a grain boundary when ω_{gb} is negative, or $\frac{\Delta H^{\mathrm{seg}}}{\Delta H^{\mathrm{mix}}} > 1$ for our alloy systems. An ideal case is when solute segregation at grain boundaries creates the lowest energy state among all bond types, ultimately making a nanoscale grain structure the ground state. This condition is characterized by $\omega_{\mathrm{gb}} + \frac{2\Omega^{\mathrm{A}}\gamma_0^{\mathrm{A}}}{zt} < 0$ and highlighted in green in Fig. 2. The representative alloy D in this "classical nanostructured" region has bond energies that are ordered $E_{\mathrm{c}}^{\mathrm{AB}} > (E_{\mathrm{gb}}^{\mathrm{AA}} = E_{\mathrm{gb}}^{\mathrm{BB}}) > (E_{\mathrm{c}}^{\mathrm{AA}} = E_{\mathrm{c}}^{\mathrm{BB}}) > E_{\mathrm{gb}}^{\mathrm{AB}}$; solute segregated grain boundaries are preferred over bulk phase separation, and undecorated grain boundaries over bulk solid solution.

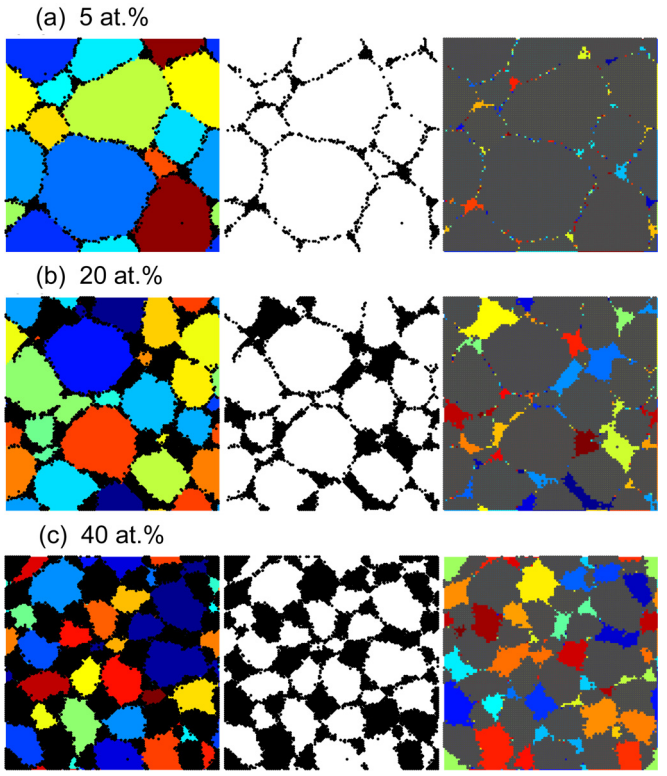

FIG. 6. (Color online) Duplex nanocrystalline structures from system "C" at 500 °C with (a) 5 at.%, (b) 20 at.%, and (c) 40 at.% solute content from a 100 × 100 × 6 BCC lattice with $\Delta H^{\text{mix}} = 50$ kJ/mol and $\Delta H^{\text{seg}} = 65$ kJ/mol. The solute atoms are presented in black in the first and second columns with and without the grain structure, respectively. The grain structure of the solute-rich regions is displayed with solvent atoms highlighted in gray in the third column. The solute-rich regions remain crystalline at all concentrations.

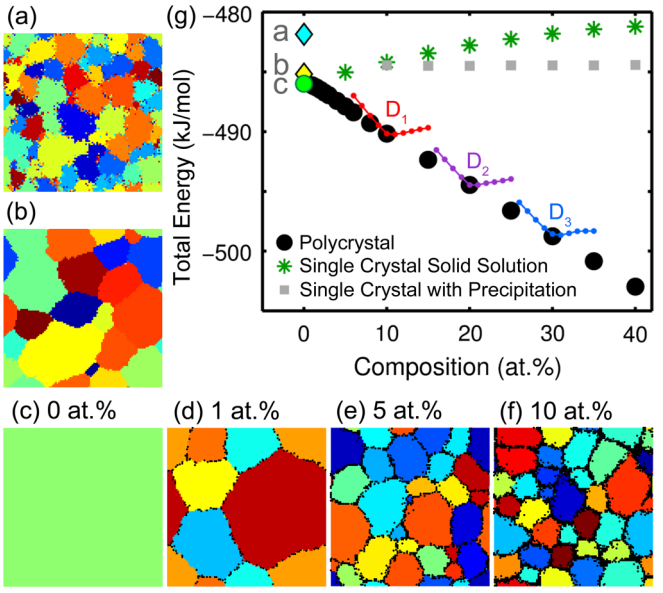

FIG. 7. (Color online) The structures and total energy of system "D" with 0–40 at.% solute. For the unalloyed material, the system energy reduces upon cooling from (a) a fine-grained polycrystalline structure to (b) a coarse-grained structure, and finally, (c) a single crystal in equilibrium. The equilibrated structures are provided for (d) 1 at.%, (e) 5 at.%, and (f) 10 at.% alloys, along with (g) an inverse relationship between the total system energy and the solute content. With increasing solute content, the system energy is lowered and a smaller average grain size can be accessed. The energies of alloys with a static grain structure but varied solute concentration are also provided, indicating that for a grain structure there is a certain global concentration needed for the system energy to be minimized. The energies of single-crystal structures are provided as a reference; for a single-crystal structure, bulk precipitation emerges at 10 at.% composition and provides lower-energy states compared to a single-crystal solid solution. Simulations are performed on a 100 × 100 × 6 BCC lattice with $\Delta H^{\text{mix}} = 20$ kJ/mol, $\Delta H^{\text{seg}} = 65$ kJ/mol, and $T = 500$ °C.

Some typical nanostructures that emerge in system D are shown along the bottom of Fig. 7, in panels (d)–(f). Here, we observe polycrystalline structures that are clearly decorated at the boundaries with solute, and as more solute is available, the grains become finer to accommodate it. This is classical nanostructure stabilization of the kind envisioned by Weissmuller [1,2], Kirchheim [9,10], and in our group's prior work [13–15]. The notion that such nanostructures are formally system ground states presents an interesting alternative to conventional bulk materials thermodynamics, and proposes a major correction to, e.g., the assembly of binary alloy phase diagrams. As such, it is instructive to examine the energetics and structural degrees of freedom of such materials with the present MC model, where we can independently manipulate the structural constituents and explore the nature of these nanocrystalline ground states.

A. System energy

First, we compare the structure and total energy of alloy D after equilibration at 500 °C with those of the unalloyed material under the same conditions. The sequence of panels (a)–(c) in Fig. 7 shows the evolution of the unalloyed structure upon cooling. As expected, the grain structure is initially a fine grained polycrystal (a) that coarsens (b) until the single-crystal ground state is achieved (c) over the course of the cooling process. In panel (g), the total system energy is shown for these structures, and the monotonic drop from points "a" to "c" corresponds to the coarsening process; the total energy at point "c" represents the lowest energy that can be achieved in the unalloyed condition.

Next, we consider the addition of solute atoms. Before considering the nanocrystalline systems, it is instructive to consider the energy of a single-crystalline system that is alloyed; such systems are produced by the same equilibration process but with only a single (unchanging) grain number used for the whole MC lattice. The asterisk and square data points in Fig. 7(g) show the energy of such single-crystalline alloys. Even though the single-crystalline alloys are equilibrated without the presence of grain boundaries, solute precipitation is still a possible competing bulk state. Given their equal enthalpy of mixing, the single-crystalline behaviors of alloy D are identical to those of alloy A shown earlier in Fig. 5(a). We observe precipitation of solute emerging at 10 at.% concentration in

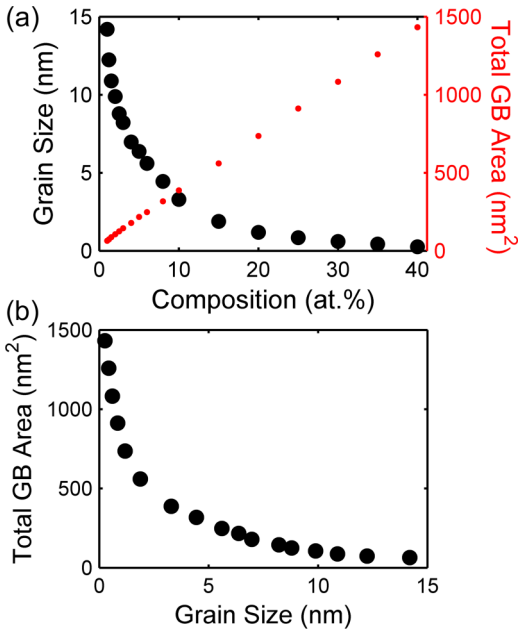

FIG. 8. (Color online) (a) Inverse relationship between average grain size and solute content in the classical nanostructured alloy D with 1–40 at.% solute concentration at 500 °C, shown with the associated change in total grain boundary area. (b) The total grain boundary area increases as the average grain size decreases with solute addition.

both systems, with a plateau of lower-energy states from precipitation presented by the square data points. The energies of a single-crystalline random solid solution are also provided by the asterisk data points in Fig. 7(g) as a reference. Their values increase slightly with alloying level; this is expected since the alloy in question has a modest positive enthalpy of mixing.

Compared with any of the above results on alloyed or unalloyed single crystals, the system energy can be lowered even further to achieve unique ground states when the grain structure is allowed to remain polycrystalline in the alloyed systems. The series of panels (d)–(f) show the resulting equilibrated structures, which, as noted earlier, are characterized by grain boundary segregation. What is clear now by comparison of the data in Fig. 7(g), is that these structures are of lower energy than any single-crystal solid solution in this alloy system; these are thermodynamically stable nanocrystalline structures in which grain growth at constant composition is an energy raising proposition.

The black data points in panel (g) show a linear decrease in energy with composition, which is in line with analytical calculations in Ref. [17]. What is more, these structures [cf. Figs. 7(d), 7(e), and 7(f)] exhibit smaller average grain sizes with increasing solute content. This is made more explicitly clear in Fig. 8(a), which shows an inverse relationship between grain size and composition as expected in this regime; solute excess drives the system toward grain boundary retention rather than solvation or precipitation. Here, the average grain size is calculated from the diameter of volume-equivalent cylinders and converted to the nanometer scale using the lattice parameter of 3.16 Å.

B. Reduction in grain boundary formation energy

As noted in the introduction, the equilibrium condition for closed alloy systems with grain boundaries is the one in which the total system energy is minimized with respect to any change in grain size, i.e., $\frac{dG}{dA} = 0$. The equilibrated structures in Figs. 7 and 8 all must satisfy this condition. As also noted in the introduction, there is opportunity for confusion in closed systems because $\frac{dG}{dA}$ is not equal to γ, and both quantities are occasionally called "grain boundary energy." To clarify the relationship between these variables and to more clearly elaborate their circumstances in equilibrium, we proceed to directly evaluate them from the simulated structures.

We call γ the "grain boundary formation energy," and it is the difference between the energy of a grain boundary structure and that of a perfect crystal normalized by the total grain boundary area [14,35]:

$$\gamma = \frac{\Delta E_{\text{defect}} - \Delta E_{\text{ideal}}}{A_{\text{defect}}}, \tag{12}$$

where ΔE_{defect} and ΔE_{ideal} are, respectively, the formation energies of the polycrystal and a single crystal and A_{defect} is the total grain boundary area in the polycrystal. The single crystal must possess the same chemical ordering (chemical potentials) as the defected structure such that the energy difference results only from topological defects [14]. By replacing all grain numbers in the equilibrated alloy structure with a single value, a single crystal with the same chemical distribution as the original alloy structure can be obtained, based on whichΔE_{ideal} may be calculated. The total grain boundary area can be obtained by replacing all atoms in the alloy with the solvent, thus creating a pure polycrystal with the identical grain structure, and calibrating it using Eq. (12) with the formation energy of a pure single crystal (as ΔE_{ideal}) and the grain boundary formation energy of the pure metal. After obtaining ΔE_{ideal} and A_{defect} of the alloy, the total energy of the equilibrated alloy is used as ΔE_{defect} and the alloy grain boundary formation energy can be calculated.

Upon increasing the solute content, a higher fraction of grain boundaries exists in equilibrium to accommodate the solute, and Fig. 8 shows a monotonic increase in the total grain boundary area, or A_{defect}, as the concentration increases [Fig. 8(a)], or as the grain size is refined [Fig. 8(b)]. The reduction of the grain boundary formation energy is presented in Fig. 9, on both linear (a) and logarithmic (b) scales with composition. On the logarithmic scale, the alloy grain boundary formation energy displays a nearly linear trend with composition, as expected (at least in the dilute limit) from Eq. (4). The grain boundary specific solute excess, Γ, is estimated from the best fit line in Fig. 9(b) to be approximately 36–49 atoms/nm^2, which is a physically reasonable value.

At 0 at.% concentration, the grain boundary formation energy is 1.1 J/m^2, which matches the input γ_0 value. After alloying, the grain boundary formation energy is reduced significantly *below* zero. It has been pointed out in a discussion of Kirchheim and Gottstein [3,4] that for closed systems, the first two terms on the right-hand side of Eq. (3) are positive but their magnitudes are small. In order to attain equilibrium ($\frac{dG}{dA} = 0$), the grain boundary formation energy, γ, then must be negative. The negative values of γ obtained in Fig. 9

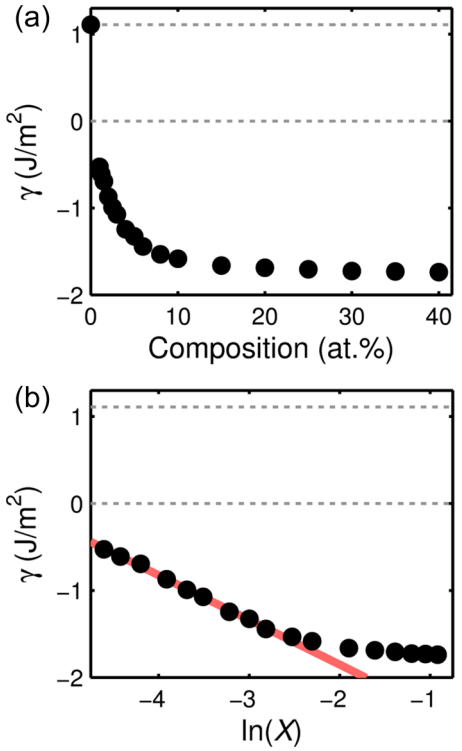

FIG. 9. (Color online) Reduction in grain boundary formation energy with solute addition. In the classical nanostructured alloy D, the grain boundary formation energy is reduced to a negative value, indicating that these nanocrystalline alloys are lower in energy than their single-crystalline counterparts. The variation between the effective grain boundary formation energy and $\ln(X)$ is almost linear as expected at dilute concentrations. The single-component and zero grain boundary formation energy are noted by the dotted lines.

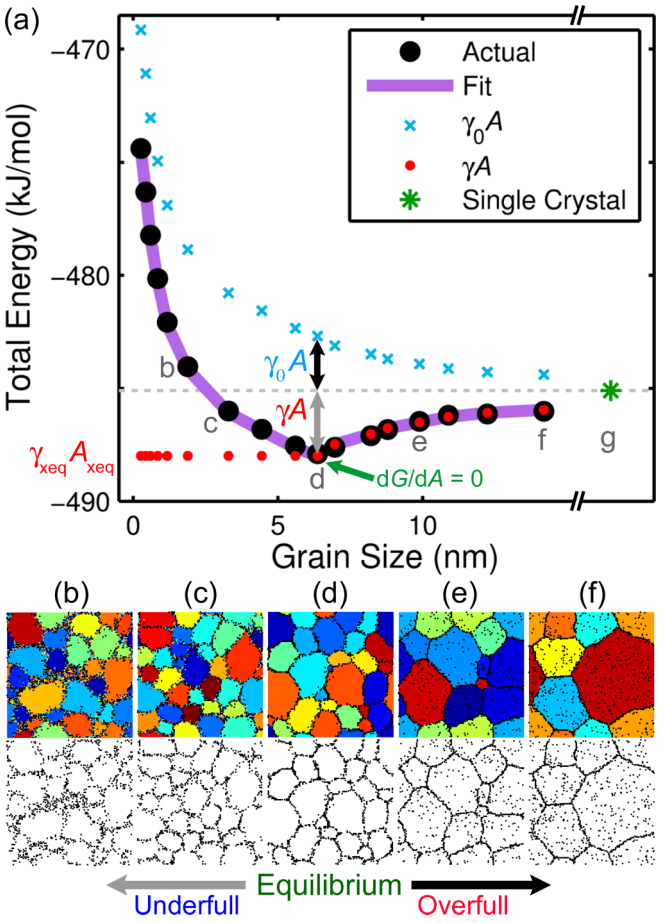

FIG. 10. (Color online) (a) Total system energy of 5 at.% classical nanostructured alloys from system "D" with various predetermined average grain sizes. The system energy is minimized at point "d" with the grain structure obtained from the equilibrium 5 at.% alloy. The structures with smaller or larger average grain sizes are observed to have higher energy with under-full and over-full solute segregated grain boundaries, respectively. With the energy of a single-crystalline solid solution under the same conditions, denoted by "g," as the reference state, the energies of alloys with equilibrium and over-full grain boundaries are lowered by $\gamma_{\text{xeq}}A$ via grain boundary segregation, while the alloys with under-full grain boundaries possess both energy increment and penalty of the magnitude $\gamma_{\text{xeq}}A_{\text{xeq}} + \gamma_0(A - A_{\text{xeq}})$. The structures of 5 at.% alloys after equilibration are provided for the original grain structures from (b) 15 at.%, (c) 10 at.%, (d) 5 at.%, (e) 2 at.%, and (f) 1 at.% alloys. Simulations are performed on a 100 × 100 × 6 BCC lattice with $\Delta H^{\text{mix}} = 20$ kJ/mol, $\Delta H^{\text{seg}} = 65$ kJ/mol, and $T = 500$ °C.

are thus expected. The implication of a negative alloy grain boundary formation energy is not that unchecked creation of grain boundaries is preferable, but rather that a very specific solute-segregated grain boundary configuration can reduce the system energy according to Eq. (1). Such configuration depends in detail on the solute concentration according to Eq. (4). The fraction of decorated grain boundaries in the equilibrium state is limited by the amount of solute available in the system. Any grain boundary area created beyond the capacity of solute to stabilize them would annihilate in equilibrium because of the energy penalty from $\gamma_0 A$.

To further elucidate this concept, we use our simulation to compare the total energy of alloy D when the composition is fixed at 5 at.% but the grain size is varied away from the equilibrium value. This is accomplished by using equilibrated grain structures obtained from those in Fig. 7, at a variety of compositions that effect different grain sizes (Fig. 8). These structures then have their chemical composition reassigned to a value of 5 at.% solute, before the structures are equilibrated isothermally at 500 °C, while fixing the grain structure. In this way we fix a nanoscale grain size and explore the preferred solute configuration on that structure, with results as shown in Fig. 10.

The solid data points in Fig. 10 show the raw output of these simulations, giving the total system energy as a function of grain size at fixed composition. With no precipitation and therefore a negligible change in entropy, the slope of this data is $\frac{dG}{dD}$, with D the grain size, and is related to $\frac{dG}{dA}$ as $\frac{dG}{dA} = \frac{dG}{dD}\frac{dD}{dA}$, with the functional form between A and D presented in Fig. 8(b). These data show an energy landscape that is reminiscent of those proposed by Weissmuller [1,2] and others [15], which decreases to a minimum value before rising again. Even though all of the obtained final structures are energy minimized with respect to the chemical distributions in their present grain structures, the true minimum energy can only be achieved at a specific grain size, shown in Fig. 10(d), where the grain structure is obtained from the equilibrium 5 at.% alloy structure, which is exactly the point where $\frac{dG}{dD} = \frac{dG}{dA} = 0$.

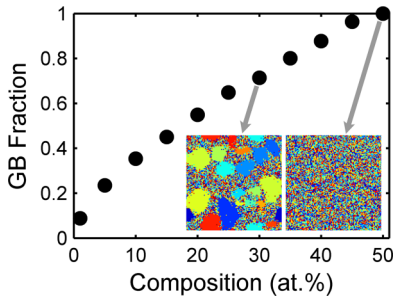

FIG. 11. (Color online) The grain boundary fraction increases with solute content in the classical nanostructured alloys. The grain structures, provided in the insets, are composed of a large volume fraction of grain boundaries at high solute compositions and eventually become all intergranular at 50 at.%.

When a grain is smaller than the equilibrium grain size, there is an energy excess in grain boundaries that are not decorated by the solute and therefore exist in a high-energy state; grain growth towards the equilibrium value is preferred. On the other hand, when the average grain size falls above the equilibrium value, all grain boundaries are decorated but there are grain interior bonds that could exist in an otherwise lower-energy solute-segregated grain boundary configuration, if there only were grain boundary sites to accept them. The balance between under-full and over-full grain boundary networks results in a specific equilibrium grain size. The fine-grained equilibrium structure in Fig. 10(d) possesses a lower energy than its single-crystalline counterpart, denoted by the asterisk labeled "g."

With a single crystal as the reference state, grain refinement raises the system energy by $\gamma_0 A$ from the increase in total grain boundary area, and when alloyed, counteracted by γA from the reduced equilibrium grain boundary formation energy. Based on the free energy expression in Eq. (1) and a single-crystal solid solution with energy $\Sigma\mu_i N_i$ as the reference state, these two terms ($\gamma_0 A$ and γA) are isolated and plotted in Fig. 10 along with the actual system energy obtained from our simulated alloy structures. For grain sizes above the equilibrium value, all grain boundaries are stabilized; the grain boundary formation energy γ is thus the equilibrium grain boundary formation energy of the 5 at.% alloy and A is the total grain boundary area at each grain size. However, for the grain sizes below the equilibrium value, only a fraction of grain boundaries are decorated and stabilized by the solute, and therefore γA is fixed to the value of the equilibrium 5 at.% alloy. The remaining grain boundaries are undecorated and possess the energy penalty from γ_0. The overall energy is thus $G = \Sigma\mu_i N_i + \gamma_{\text{xeq}} A_{\text{xeq}} + \gamma_0(A - A_{\text{xeq}})$, where the subscript denotes the equilibrium concentration (5 at.% in this case). The resulting energy function provides a good fit for the total energy of our alloy structures.

As a complementary line of logic to the above, a static grain structure can be equilibrated with the solute composition varied. The subplots in Fig. 7(g) labeled "D_1," "D_2," and "D_3" represent the energies of alloys with a fixed grain structure but different solute concentrations specified by the x axis. The results show three energy minima that align with the equilibrium data points in black, suggesting that for a certain grain structure (or its representative D), there is a specific global solute concentration needed to achieve grain stability. The two types of energy minima, with varying X at a fixed D in Fig. 7(g) and with varying D at a fixed X in Fig. 10, are in line with the one-to-one relationship between global solute concentration and equilibrium grain size presented earlier in Fig. 8(a) and the consequent control of grain size via solute concentration in these classical nanostructured alloys.

Finally, we note that with solute-segregated grain boundaries being preferred over phase separation, and with an excessive amount of grain boundaries induced by the solute, the structures of alloy D from the classical nanocrystalline regime can display an amorphouslike structure at the highest solute concentrations. Due to the nature of our fixed lattice simulation, an amorphous structure is not explicitly captured as a state of disordered atomic packing, but rather as a system in which individual grains are so small as to defy definition as crystals (i.e., no larger than a few atoms). This is captured by a high volume fraction of atoms coordinating grain boundaries, as shown quantitatively in Fig. 11. All atoms have at least one grain boundary bond at 50 at.% concentration. This amorphouslike structure is in line with the analytical thermodynamic calculations from Refs. [2] and [17], which suggested that there is a terminal concentration at which a nanocrystalline state can exist, and above which the grain size refines to the order of the grain boundary thickness and an amorphous phase can emerge close to the equiatomic concentration.

V. CONCLUSIONS

We have developed a Monte Carlo simulation for the purpose of investigating polycrystalline alloys in which both the chemical configuration and grain structure are allowed to vary. The model is built in such a way that classical McLean-type grain boundary segregation and regular solution mixing are recovered in the proper limits. By using the simulation to visualize grain-atomic structures and study alloy energetics, grain stability is explored in phase-separating binary alloys with the following findings. (1) Grain boundary segregation states in some alloys can be energetically favorable compared to any competing bulk states, and therefore a polycrystalline structure is the system's ground state. (2) The distinction between what we call the "grain boundary formation energy" γ and the "grain boundary area potential" $\frac{dG}{dA}$ in a closed system is clarified using simulation results. Whereas these two terms are both equivalent and called "grain boundary energy" in an open system, in a closed system γ is related to the energy change caused by topological defects and $\frac{dG}{dA}$ is related to the equilibrium grain size attainment. (3) Upon alloying, a negative γ is physically plausible, and stability against both grain growth and phase separation can be achieved when γ is negative and $\frac{dG}{dA} = 0$ in closed systems. (4) The free energy landscape and γ can both be modified via solute addition, as observed in different types of nanostructure behaviors with alloy material parameters (ΔH^{mix} and ΔH^{seg}) and control of equilibrium grain size via solute concentration.

ACKNOWLEDGMENT

This work was supported by the US Army Research Office, under Grant No. W911NF-09-1-0422.

[1] J. Weissmüller, Nanostruct. Mater. **3**, 261 (1993).
[2] J. Weissmüller, Mater. Sci. Eng.: A **179**, 102 (1994).
[3] R. Kirchheim, Scr. Mater. **55**, 963 (2006).
[4] G. Gottstein and L. Shvindlerman, Scr. Mater. **55**, 965 (2006).
[5] P. C. Millett, R. P. Selvam, S. Bansal, and A. Saxena, Acta Mater. **53**, 3671 (2005).
[6] P. C. Millett, R. P. Selvam, and A. Saxena, Acta Mater. **55**, 2329 (2007).
[7] Y. Purohit, L. Sun, O. Shenderova, R. O. Scattergood, and D. W. Brenner, Acta Mater. **59**, 7022 (2011).
[8] R. Kirchheim, Acta Mater. **50**, 413 (2002).
[9] R. Kirchheim, Acta Mater. **55**, 5129 (2007).
[10] R. Kirchheim, Acta Mater. **55**, 5139 (2007).
[11] D. L. Beke, C. Cserhati, and I. A. Szabo, J. Appl. Phys. **95**, 4996 (2004).
[12] P. C. Millett, R. P. Selvam, and A. Saxena, Acta Mater. **54**, 297 (2006).
[13] A. J. Detor and C. A. Schuh, Acta Mater. **55**, 371 (2007).
[14] A. J. Detor and C. A. Schuh, Acta Mater. **55**, 4221 (2007).
[15] J. R. Trelewicz and C. A. Schuh, Phys. Rev. B **79**, 094112 (2009).
[16] T. Chookajorn, H. A. Murdoch, and C. A. Schuh, Science **337**, 951 (2012).
[17] H. A. Murdoch and C. A. Schuh, Acta Mater. **61**, 2121 (2013).
[18] P. S. Sahni, D. J. Srolovitz, G. S. Grest, M. P. Anderson, and S. A. Safran, Phys. Rev. B **28**, 2705 (1983).
[19] G. S. Grest, M. P. Anderson, and D. J. Srolovitz, Phys. Rev. B **38**, 4752 (1988).
[20] A. Mazor, D. J. Srolovitz, P. S. Hagan, and G. B. Bukiet, Phys. Rev. Lett. **60**, 424 (1988).
[21] R. LeSar, R. Najafabadi, and D. J. Srolovitz, Phys. Rev. Lett. **63**, 624 (1989).
[22] P. Bruschi, P. Cagnoni, and A. Nannini, Phys. Rev. B **55**, 7955 (1997).
[23] N. Ono, K. Kimura, and T. Watanabe, Acta Mater. **47**, 1007 (1999).
[24] D. Raabe, Acta Mater. **48**, 1617 (2000).
[25] J. Creuze, F. Berthier, R. Tétot, and B. Legrand, Phys. Rev. Lett. **86**, 5735 (2001).
[26] E. Holm and C. Battaile, JOM **53**, 20 (2001).
[27] K. N. Tu, A. M. Gusak, and I. Sobchenko, Phys. Rev. B **67**, 245408 (2003).
[28] A. E. Lobkovsky, A. Karma, M. I. Mendelev, M. Haataja, and D. J. Srolovitz, Acta Mater. **52**, 285 (2004).
[29] Y. Purohit, S. Jang, D. L. Irving, C. W. Padgett, R. O. Scattergood, and D. W. Brenner, Mater. Sci. Eng.: A **493**, 97 (2008).
[30] J. Gruber, H. M. Miller, T. D. Hoffmann, G. S. Rohrer, and A. D. Rollett, Acta Mater. **57**, 6102 (2009).
[31] M. D. Leblanc, M. L. Plumer, J. P. Whitehead, and J. I. Mercer, Phys. Rev. B **82**, 174435 (2010).
[32] K.-J. Ko, A. D. Rollett, and N.-M. Hwang, Acta Mater. **58**, 4414 (2010).
[33] Y. Purohit, L. Sun, D. L. Irving, R. O. Scattergood, and D. W. Brenner, Mater. Sci. Eng.: A **527**, 1769 (2010).
[34] B. Sadigh, P. Erhart, A. Stukowski, A. Caro, E. Martinez, and L. Zepeda-Ruiz, Phys. Rev. B **85**, 184203 (2012).
[35] R. Najafabadi, H. Wang, D. J. Srolovitz, and R. LeSar, Scr. Mater. **25**, 2497 (1991).